



# Separation of Damping and Velocity Strain Dependencies using an Ultrasonic Monochromatic Excitation

C. Mechri, M. Scalerandi, Mourad Bentahar

## ► To cite this version:

C. Mechri, M. Scalerandi, Mourad Bentahar. Separation of Damping and Velocity Strain Dependencies using an Ultrasonic Monochromatic Excitation. *Physical Review Applied*, 2019, 10.1103/PhysRevApplied.11.054050 . hal-02462789

HAL Id: hal-02462789

<https://univ-lemans.hal.science/hal-02462789>

Submitted on 31 Jan 2020

**HAL** is a multi-disciplinary open access archive for the deposit and dissemination of scientific research documents, whether they are published or not. The documents may come from teaching and research institutions in France or abroad, or from public or private research centers.

L'archive ouverte pluridisciplinaire **HAL**, est destinée au dépôt et à la diffusion de documents scientifiques de niveau recherche, publiés ou non, émanant des établissements d'enseignement et de recherche français ou étrangers, des laboratoires publics ou privés.

# Separation of Damping and Velocity Strain Dependencies using an Ultrasonic Monochromatic Excitation

C. Mechri,<sup>1,2</sup> M. Scalerandi,<sup>3,\*</sup> and M. Bentahar<sup>1,4</sup>

<sup>1</sup> LAUM, CNRS, Université du Maine, Le Mans, France

<sup>2</sup> CTTM, 20 Rue Thals de Milet, Le Mans, France

<sup>3</sup> DISAT, Condensed Matter Physics and Complex Systems Institute, Politecnico di Torino, Torino, Italy

<sup>4</sup> ENSIM, Université du Maine, Le Mans, France



(Received 2 July 2018; revised manuscript received 14 March 2019; published 20 May 2019)

Precise knowledge of the dependence of elastic modulus and  $Q$  factor on the amplitude of excitation is a prerequisite for the development and validation of models to explain the hysteresis observed in quasistatic experiments for various media, i.e., the different deformations at the same applied stress observed when stress change rate is positive or negative. Separation of different contributions to dynamic nonlinearity (e.g., those due to nonequilibrium effects, often termed conditioning) and independent estimation of nonlinearities originated by the strain dependence of velocity and the damping factor are required, which is often not possible with standard approaches. Here we propose and validate a method that, measuring the response of a sample to a monochromatic excitation at different amplitudes, allows fast, continuous, and quasi-real-time monitoring of the dependence of the material elastic properties on amplitude: dynamic elastic modulus (related with velocity through density) and  $Q$  factor of the mechanical resonances (related with wave-amplitude attenuation parameters).

DOI: 10.1103/PhysRevApplied.11.054050

## I. INTRODUCTION

Understanding the physical origin of elastic nonlinearity and hysteresis in consolidated [1–4], unconsolidated [5], or damaged [6] granular media requires the separation of modulus- and attenuation-coefficient strain dependencies, which cause a nonlinear response of the medium to an ultrasonic excitation (nonlinear dependence of stress on strain). For the sake of simplicity, in the following we use the term velocity or damping nonlinearity to indicate the sample nonlinearity due to the strain dependencies of the two variables. The role of conditioning, memory and relaxation [7,8], i.e., the dependence of velocity and  $Q$  factor on time and on maximum strain (history), should also be clarified and their effect decoupled from classical effects due to the actual amplitude dependence of investigated physical quantities [9].

Several nonlinear indicators [10–15], i.e., measurable quantities, which are analyzed as a function of strain amplitude, are used to quantify nonlinearity, but often provide a measurement in which effects resulting from nonlinear attenuation and nonlinear elasticity are mixed up. Also the definition of the  $Q$  factor used, e.g., in nonlinear resonant ultrasound spectroscopy [16–19], is critical, due to distortions of the resonance curve, which, e.g., is

no longer symmetric. A  $Q$  factor could always be defined from half width at half height, but its link with the damping coefficient is no longer well defined. At the same time, due to the intrinsic time required for acquisition (which might be of the order of tens of seconds when averaging is needed), monitoring early stages of conditioning and relaxation is often problematic [7,8].

Finally, we recall that most commonly the nonlinearity of a sample is classified according to a power-law dependence of the nonlinear indicator on a not univocally specified “amplitude” of excitation [20,21], which often is the strain amplitude evaluated at the same spatial position where the signal is measured. Different components of the strain field are neglected and often the longitudinal component only (to which the detecting sensor is more sensible) is considered, which is correct when one-dimensional (1D) geometries are considered.

Furthermore, measurements, in general, provide an estimate of the nonlinear indicator resulting from the global effect of a particular wave, e.g., one (or more) cycle of a periodic sinusoidal wave. In reality, however, velocity and damping vary continuously with time, following the evolution of the wave itself and their “average” estimation over a cycle, might be misleading in the validation of models based on physical assumptions [22–24]. The dynamic modulus can indeed be measured using the dynamic acoustoelastic testing (DAET) approach [25–28],

\*marco.scalerandi@infm.polito.it

which tracks nonlinearity in time as a function of the so-called pump amplitude. Even in this case, it is however difficult to estimate correctly the  $Q$  factor of the material and the experimental configuration might be complex to implement.

The goal of this paper is to propose and validate an experimental technique to measure the dependence of velocity and damping on amplitude, with an exact analytical separation of the contributions. In this paper, measurements make use of monochromatic waves at varying amplitude, in contrast with resonance frequency measurements in which sweeps or a succession of several monochromatic waves at increasing frequency are needed. The proposed method is therefore easy to implement and acquisitions can be extremely fast, continuous, and almost in real time (including averaging). Finally, the monochromatic wave can be excited close to resonance in order to provide sufficient energy to excite and easily probe the hidden nonlinearity within complex media.

## II. THEORY

### A. Linear solution derivation

Let us consider a 1D elastic medium, in which wave propagation, considering negligible attenuation due to external factors (e.g., friction over air), is governed by elasticity and internal friction [29–31]:

$$\rho \frac{\partial^2 u}{\partial t^2} - \psi \frac{\partial^3 u}{\partial x^2 \partial t} = S \frac{\partial^2 u}{\partial x^2}. \quad (1)$$

Depending on the forcing, the variable  $u(x, t)$  could be a longitudinal or transverse (or both) displacement. In the cases considered in the experimental part, transducers always excite and detect longitudinal displacements. In the above equation,  $\rho$  is density,  $\psi$  the attenuation parameter, and  $S$  the elastic modulus (Young or shear modulus, depending on excitation).

In the case of a semi-infinite medium with a monochromatic forcing  $F(t)$  in  $x = 0$ , a possible solution is a monochromatic wave field:

$$u(x, t) = U_0 e^{-\alpha x} e^{j[\omega(t-t_0)-kx]}, \quad (2)$$

where  $\phi_0 = -\omega t_0$  and  $U_0$  are the phase and amplitude at  $x = 0$  and  $t = 0$ . The phase velocity is given by  $c = \omega/k$  and the  $Q$  factor is  $Q = \omega/\alpha c$ .

By introducing Eq. (2) into Eq. (1), we obtain a link between the modulus and attenuation parameter, the wave number  $k$ , and attenuation coefficient  $\alpha$ :

$$S = \frac{\rho \omega^2 (k^2 - \alpha^2)}{(k^2 + \alpha^2)^2}, \quad (3)$$

$$\psi = 2\alpha k \frac{\rho \omega}{(k^2 + \alpha^2)^2}.$$

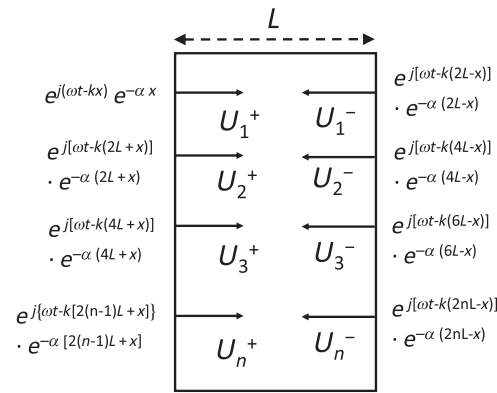


FIG. 1. Scheme of the 1D multiple reflections' vibration model.

Note that, when considering monochromatic waves, as in the present approach, the solution remains valid also in the case of a Newtonian viscosity-based attenuation term, which is often used also to describe attenuation in solids with different Kramers-Kronig relationships.

Considering a finite medium of length  $L$  with free-free boundary conditions, the analytical solution for the displacement in  $L$  can be found considering that the solution is the superposition of multiple reflections (see Fig. 1). Considering that, at free boundaries, waves (displacements) are reflected with the same amplitude as the incoming wave (while strains are reflected with a reflection coefficient  $R = -1$  due to the sign change of wave vector), it follows

$$\begin{aligned} u^+(x, t) &= \sum_{n=1}^{\infty} U_0 e^{j\{\omega t-k[2(n-1)L+x]+\phi_0\}} e^{-\alpha[2(n-1)L+x]}, \\ u^-(x, t) &= \sum_{n=1}^{\infty} U_0 e^{j[\omega t-k(2nL-x)+\phi_0]} e^{-\alpha(2nL-x)}, \\ u(x, t) &= u^+(x, t) + u^-(x, t). \end{aligned} \quad (4)$$

The solution at the edge of the sample ( $x = L$ ) is again a sinusoidal wave with amplitude  $A$  and phase  $\phi$ :

$$u(L, t) = A e^{j[\omega(t-t_0)+\phi]} = A e^{j(\omega t+\Phi)}, \quad (5)$$

where

$$A = \frac{U_0}{\sqrt{\cosh^2(\alpha L) - \cos^2(kL)}}, \quad (6)$$

$$\Phi = \phi_0 + \phi = \phi_0 - \arctan \left[ \frac{\tan(kL)}{\tanh(\alpha L)} \right]. \quad (7)$$

We recall that  $U_0$  is the amplitude of the solution at  $x = 0$  for a semi-infinite medium, where the phase is  $\phi_0$  [see Eq. (2)]. Thus,  $U_0$  has the meaning of the contribution to the displacement amplitude in  $x = 0$  due to the forcing induced by the transducer, which is added to the contribution to displacement (always in  $x = 0$ ) due to the multiply

reflected traveling waves. As such,  $U_0$  (and the same for  $\phi_0$ ) is a property of the transducer, which, as discussed later, can be determined only from a proper calibration procedure. If the transducer is linear, proportionality holds true for  $U_0$  in the sense that, amplifying voltage amplitude at the source of a factor  $k$ , the same amplification applies to  $U_0$  (while  $\phi_0$  is unchanged).

Details of the derivation are reported in Appendix A. In Appendix B, we show how the solution and boundary conditions look when strains are considered and the role of  $U_0$  is further clarified. As shown, the quantity  $U_0$  is also proportional to the amplitude of the driving force generated by a light transducer located at  $x = 0$ . We anticipate here that in our experiments the signals are detected at  $x = L$  with a second light transducer.

Modifications of the solution in the case of not free-free boundary conditions are discussed in Appendix C. We remark here that with the term free-free boundary conditions we indicate that the resonant frequencies in the experimental setup are practically the same as the frequencies of the fundamental modes of free oscillations, which, as discussed in Appendix C, is verified in the experiments discussed in Sec. IV.

## B. Inversion

Equations (6) and (7) can be used to extract  $k$  and  $\alpha$  from experimental data. Let us consider a 1D sample excited at one edge with a sinusoidal wave at frequency  $\omega$ . The signal at the other edge can be recorded and its amplitude  $A$  and phase  $\Phi = \phi + \phi_0$  (we recall that  $\phi_0 = -\omega t_0$ ) can be derived by fitting experimental data with a cosine function. Furthermore, calibrating the experiment as discussed in the next subsection,  $U_0$  and  $\phi_0 = -\omega t_0$  can be derived. Thus also the phase  $\phi = \Phi - \phi_0$  can be measured. Inverting Eqs. (6) and (7), we obtain the physical parameters. In particular, we have

$$c = \omega/k = \frac{\omega}{\frac{1}{L} \left[ \pi n \pm \arctan \sqrt{\frac{z}{2 \cos^2(\phi)}} \right]}, \quad (8)$$

$$\alpha = \frac{1}{L} \operatorname{artanh} \sqrt{\frac{z}{2 \sin^2(\phi)}}, \quad (9)$$

where the sign is plus if  $\phi + \phi_0 > 0$ ,  $n$  is the order of the closest mode to  $\omega$  and

$$z = -(A/U_0)^2 - \cos(2\phi) + \sqrt{1 + (A/U_0)^4 + 2 \cos(2\phi)(A/U_0)^2}. \quad (10)$$

The solution is derived in Appendix D. Once the wave number  $k$  and attenuation parameter  $\alpha$  are determined, modulus and damping factor can be derived using Eq. (3).

## C. Calibration

As discussed, a preliminary calibration of the experiment is needed to derive the amplitude  $U_0$  and the phase  $\phi_0$ , which do not coincide with those at the generator due to the presence of the circuit connected to the two transducers. To this purpose, two signals are measured at  $x = L$  when exciting the sample (at  $x = 0$ ) with two sinusoidal waves at slightly different frequencies ( $\omega_0$  and  $\omega_0 + \delta\omega$ ) at the same (linear) injection amplitude. Phases and amplitudes of the two signals are measured and, since the two frequencies are close, we can neglect dispersion in both attenuation and velocity. It follows that Eq. (9) provides a set of four equations (two for each signal and frequency), with four unknowns;  $c$ ,  $\alpha$ ,  $U_0$ , and  $\phi_0$ .

In principle, calibration is obtained measuring only two signals. For practical purposes, in order to reduce errors in the evaluation of  $U_0$  and  $\phi_0$ , the procedure can be repeated for several couples of frequencies and averaging the obtained values for  $U_0$  and  $\phi_0$ . From the experimental point of view, it should be verified that the response of the detection and acquisition system is frequency and amplitude independent. In particular, the linearity of transducers must be tested to ensure that calibration obtained at one level of excitation can be straightforwardly scaled to any amplitude. Note also that, in order to increase signal-to-noise ratio it is better to perform the calibration in a narrow frequency range around one mode.

## III. NONLINEARITY

The linear Eq. (1) and linear solution (5) are of course not valid in the exact form for nonlinear media. However, as we discuss here, they can still be used to characterize nonlinearity as the deviation from the linear behavior.

When dealing with nonlinear media in fact, velocity and damping are a function of strain, which means that, even in the simplest 1D case with longitudinal propagating waves, two considerations have to be taken into account: additional model parameters (e.g., nonlinear moduli) are needed to describe the system; velocity and damping depend implicitly on time, since strain depends on time (and also position). This leads to two major problems: if only one point can be accessed for measurements (as normally in experiments longitudinal transducers can be located only on the opposite faces of the sample) only two variables can be measured; since these two quantities are derived using signals, which have a time scale longer than one period (and the propagation path from source to receiver is of the order of the wavelength or larger), intrinsic averaging is implicit.

For several materials (mostly consolidated granular media or damaged samples), nonlinearity can not be described by a simple Taylor expansion, rather conditioning and hysteresis makes velocity (and damping) dependent not only on strain ( $\epsilon$ ), but also on the maximum

strain ( $\epsilon_{\max}$ ) to which the sample is subjected. The simpler expression to define the situation is to assume that two contributions must be considered

$$c = c_L + \delta c_{\text{neq}}(\epsilon_{\max}) + \delta c_{\text{NL}}(\epsilon). \quad (11)$$

The terms  $c_L$ ,  $\delta c_{\text{neq}}$  and  $\delta c_{\text{NL}}$  represent the linear velocity and the contribution of nonequilibrium and nonlinear terms to velocity, respectively. Here, and in the following, the same considerations that hold for damping are not discussed. Without expressions for the two functions,  $\delta c_{\text{neq}}$  and  $\delta c_{\text{NL}}$ , any further exact analytical treatment is not possible and this is not the purpose here.

The contribution to nonlinearity due to conditioning (i.e., the transition of the material to a new equilibrium state as a function of the maximum strain applied) corresponds to the transition of the material to a new linear state with different velocity, given by the first two terms in Eq. (11). Thus, as long as explicit dependence on strain [term  $\delta c_{\text{NL}}(\epsilon)$ ] is zero (small), the linear solution with an amplitude dependent  $c$  and  $\alpha$  is exact (well approximated). This is often the case [4,7,8,11,26].

As mentioned, whenever distortions of the output signal from a pure monochromatic wave are weak, i.e., for small nonlinearities and/or small amplitudes of excitation, output data can be analyzed as if the solution of an “equivalent” linear medium with velocity and damping which are different from the linear (intended as low amplitude) velocity and damping. We analyze the signals used in this study and verify that, even though there are significant nonlinear

effects, as discussed later, distortions of the signals from monochromatic waves [due to the strain-dependent part of the velocity:  $\delta c_{\text{NL}}(\epsilon)$  in Eq. (11)] are sufficiently small to allow applying our treatment.

In Fig. 2, a typical experimental signal recorded on the Berea sandstone sample is reported in red and a fitting sinusoidal function is shown in dashed blue. The monochromatic solution is an excellent approximation and only small distortions might be appreciated. A FFT analysis further confirms that higher-order harmonics are negligible. The fitting analysis is conducted on signals (always on the Berea sample) at each increasing amplitude of excitation ( $A_{\text{inp}}$ ) and the coefficient of determination  $R^2$  is calculated. Its closeness to 1 indicates the good quality of the fit, which is diminishing only slightly with increasing amplitude. Note that poorer (but still acceptable) values of  $R^2$  at lower amplitudes of the excitation are due to noise and not to signal distortions.

Whenever an analytical model expression of nonlinearity is known, an alternative to this sort of “mean-field approach” could be to calculate the solution using a perturbation approach, which can however be applied only for simple nonlinear models, e.g., the classical nonlinear model. In Ref. [36] an analytical solution is given to derive the resonance frequency shift with increasing amplitude. The advantage of these approaches is to provide an estimate of nonlinear parameters (which is not straightforward here). The disadvantage is that classical (or simplified) theories do not always describe correctly the kind of nonlinearity that is present in the material.

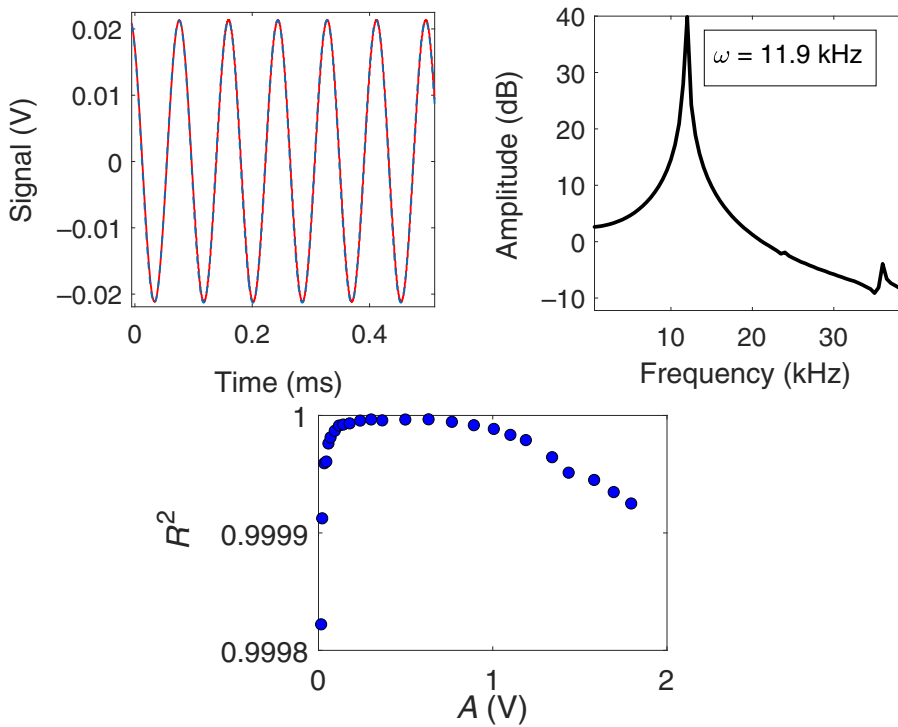


FIG. 2. Verification of the validity of a linear effective-field-like solution. Upper row: experimental signals superimposed with a fitting sinusoidal function (left); FFT of the signal (right). Lower row:  $R^2$  of the fitting sinusoidal functions at increasing amplitudes of excitation.

## IV. EXPERIMENTAL RESULTS

### A. Experimental setup

In order to discuss the proposed approach and show its validity, we consider different consolidated granular samples with a quasi-1D geometry:

(a) A Berea sandstone sample in the shape of a thin cylinder (1 cm diameter, 15 cm length). Grain size in the tested sample is of the order of tens of micrometers.

(b) A concrete sample in the shape of a cylinder (4 cm diameter and 16 cm length), drilled from a casting prepared with 340 kg of cement (CEM II A-L 42.5 R), 957 kg of sand (0–5 mm), 846 kg of gravel (5–15 mm), and 200 kg of water [water-to-cement (*w/c*) ratio is approximately equal to 0.59]. The age of the cylinder at the time of testing is about five years, thus guaranteeing that the cement hydration process is completed. In the following, we label this sample as B06.

(c) A cement-paste sample in the shape of a prism ( $3 \times 3 \times 15$  cm<sup>3</sup>). It is produced using Portland cement (CEM I 42.5N) with a *w/c* ratio of 0.3 by mass. The age of the prisms at the time of testing is about five years, thus guaranteeing that the cement hydration process is completed. Curing of the samples is done in water immersion (full saturation) for three weeks, followed by drying in ambient conditions (pressure, temperature and humidity) for additional three weeks. In the following, we label this sample as B3.

The experiment is conducted using a waveform generator (Tektronix AFG 3022B) generating ultrasonic signals defined as monochromatic waves of amplitude  $A_{\text{inp}}$  and frequency  $\omega$ . After amplification through a linear amplifier (CIPRIAN Model US-TXP-3, 200 x), signals are transmitted to an ultrasonic transducer with broadband response (i.e., an almost frequency-independent response from few kHz up to a few hundreds of kHz) acting as an emitter. The transducer is glued to the sample using Phenyl Salicylate. A second (identical) transducer is used to detect the response of the material under test and is connected to a digital oscilloscope (Lecroy 324A) for data acquisition. Signals are recorded in a short time window once stationary conditions are reached. In order to excite longitudinal modes (both transducers are working in compression mode) and to realize quasi-1D conditions, the transducers are glued on the bases of the sample.

Linearity of the acquisition system, including transducers and coupling, is verified in the frequency range from 1 up to 200 kHz, and up to excitation amplitudes of 2 V (maximum voltage before amplification). Amplitudes used in the experiment allow us to work in the nonlinear regime of the tested specimens, but still well within the limits of linearity of the setup. Linearity of the setup is tested by putting in contact the source transducer with the receiver,

glued through Phenyl Salicylate. Also, we verify that in the frequency range used in the analysis, transducers have a flat frequency response.

### B. Berea sample

#### 1. Calibration, linear velocity, and damping measurement

Experiments are conducted close to the third resonance mode, to optimize the excitation. Calibration is performed at low amplitude  $A_{\text{inp},0} = 50$  mV (before amplification), to guarantee that the sample behaves linearly. The procedure, besides allowing compensation of the effects of the transducer's transfer function (for what concerns amplitudes) and the phase shifts related to the acquisition chain, also allows evaluation of the linear velocity and *Q* factor (damping) of the considered samples.

Results of the calibration for various choices of the calibration frequency  $\omega_0$  are reported in Fig. 3. Amplitudes (*A*) and phases ( $\Phi$ ) of signals are derived fitting the experimental data with a cosine function. The derived value of the calibration parameter  $\phi_0$  is reported and has been subtracted from the measured phases  $\Phi$  to obtain the actual phase shift  $\phi$  between input ( $x = 0$ ) and output ( $x = L$ ). In (a) and (b) it can be evinced that calibration frequencies are around a resonance mode and that the phase, after correction due to calibration is 0 when the calibration frequency coincides with the third resonance mode. The fundamental resonance frequency is reported for reference. The obtained calibration parameter  $U_0$  and the estimated velocities and damping together with their averaged values are reported in (c), (d), and (e), and *c* and *Q* agree well with data from the literature [37,38]. For validating calibration, it is important to note that in a small frequency range around one resonance mode results are independent from the chosen calibration frequency. Distance correlation coefficients [39] are 0.37, 0.33, and 0.42 for  $U_0$ , *c*, and  $\alpha$ , respectively.

To further validate the calibration, independent measurements are performed: velocity is determined by cross-correlating the TOF and damping is measured with a reverberation experiment (deriving the damping coefficient from the exponential decay of the signal during reverberation). Results, shown with a red line, are in excellent agreement with those obtained with the approach presented in this paper, thus providing a proof of the validity of the free-free boundary conditions used to derive the solution. Indeed, the accuracy is of less than 1%, if defined as the difference between measured values (red line) and average of the calibration result values. Even considering the maximum distance between the red line and calibration results, accuracy is high for velocity and still less than 10% for  $\alpha$ . Fluctuations in velocity (about one per thousand) and damping (a few percent) are compatible with the order of magnitude of experimental errors (and their propagation)

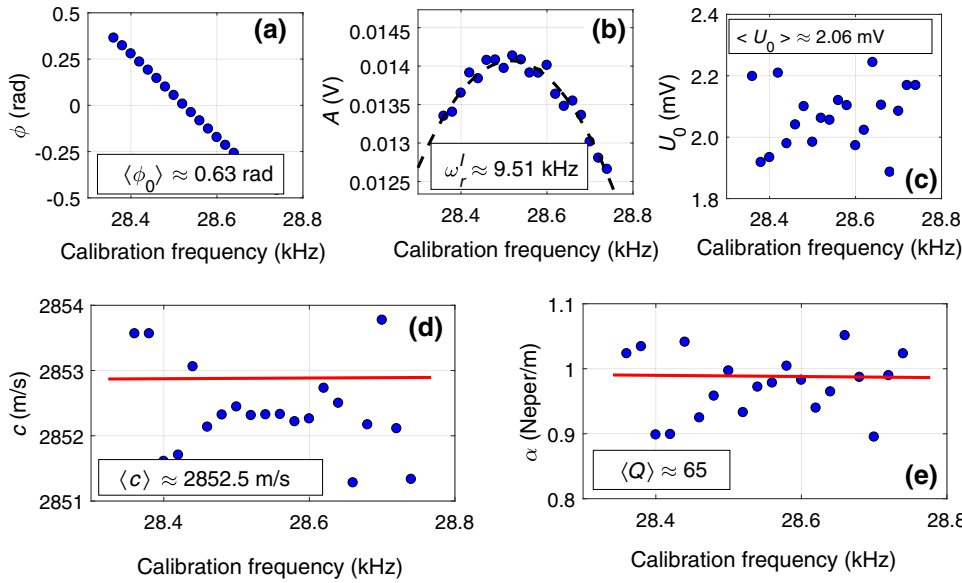


FIG. 3. Results of the calibration procedure performed. All quantities are reported as a function of the calibration frequency. (a) Phases ( $\phi = \Phi - \phi_0$ ); (b) amplitudes ( $A$ ); (c) calibration amplitude ( $U_0$ ); (d) estimated velocity; (e) estimated damping. Red lines in the last two subplots represent the values measured in independent experiments using TOF observations and reverberation decay.

and in any case are much smaller than nonlinear effects measured on the analyzed samples.

## 2. Nonlinearity

Once calibration is performed, measurements can be repeated, choosing one frequency only, at increasing amplitude of excitation:  $A_{\text{inp},i} = m_i A_{\text{inp},0}$  ( $i = 1, \dots, n$ ). In our experiments, we increase input amplitude up to 2 V (before amplification), i.e.,  $m_n = 40$ . As mentioned above, if transducers are linear the calibration parameter  $U_0$  scales linearly with input amplitude, thus calibration should not be repeated. In all cases, since we are working at low strains (less than  $10^{-7}$ , estimating repeating measurements at the largest amplitude of excitation and detecting output signals using a laser Doppler vibrometer), distortions of signals are minimal (see Fig. 2), thus fitting data with a cosine function to obtain phases and amplitudes is meaningful and, after inversion using Eq. (9) provides an effective velocity and damping for each amplitude.

The goal of such an analysis is to plot, as a function of the strain, the relative variations of velocity  $c$  and damping  $\alpha$  with respect to their linear values. Here the definition of strain is not straightforward, since the strain is a function of position (along the sample) and time. Thus, as in all other methods based on the measurement of a global variable (e.g., resonance frequency), the output signal (for each input amplitude) is the result of the propagation of the wave in a material with nonconstant strain. It is beyond the scope of this paper discussing whether the optimal estimation of the strain is the maximum strain generated by the propagating wave (e.g., in the center of the sample, if we are at resonance) or the average over time and space of the strain squared or other options.

In this paper, we use the strain definition adopted in most of the literature (when transducers are at one edge of a 1D

sample): for recent works see, e.g., [42–44]. Depending on the variable to which the transducers are sensitive, “the strain is defined by dividing the peak velocity measured by the sample’s longitudinal wave speed” [42] or as the acceleration amplitude at resonance divided by  $8\pi L\omega^2$ , where  $L$  is the sample length [43]. Our sensors are sensitive to displacements, i.e., the detected voltage  $V_{\text{out}}$  is proportional to displacement. Being the time signal a sinusoidal function (with excellent approximation as discussed before), by time deriving the signal we obtain the velocity amplitude as proportional to  $\omega V_{\text{out}}$  and the acceleration amplitude as proportional to  $\omega^2 V_{\text{out}}$ . Thus applying the two definitions of the strain  $\epsilon$  given above, we obtain

$$\begin{aligned}\epsilon &\propto \omega V_{\text{out}}/c = kV_{\text{out}}, \\ \epsilon &\propto \omega^2 V_{\text{out}}/(8\pi L\omega^2) = kV_{\text{out}}/(8\pi^2),\end{aligned}\quad (12)$$

where we use the relation  $\lambda = 2\pi/k = 2L$ , which is valid at resonance.

The strain, determined with the above expressions, is thus proportional through the wave number to the detected voltage. Furthermore, as shown in the literature (see, e.g., [33]), the strain close to the resonance is characterized by an approximate sinusoidal space profile (neglecting distortions due to attenuation):

$$\epsilon(x, t) = Ak \sin(\pi x/L)e^{j\omega t}, \quad (13)$$

where  $A$  is the displacement amplitude in  $x = L$ . Thus, the quantity  $kV_{\text{out}}$  is also proportional to the maximum strain. Finally, we also observe that the strain is often considered as a quantity directly proportional to the output acceleration (equivalent to what is proposed here but with a frequency-dependent proportionality constant): see, e.g., [45].

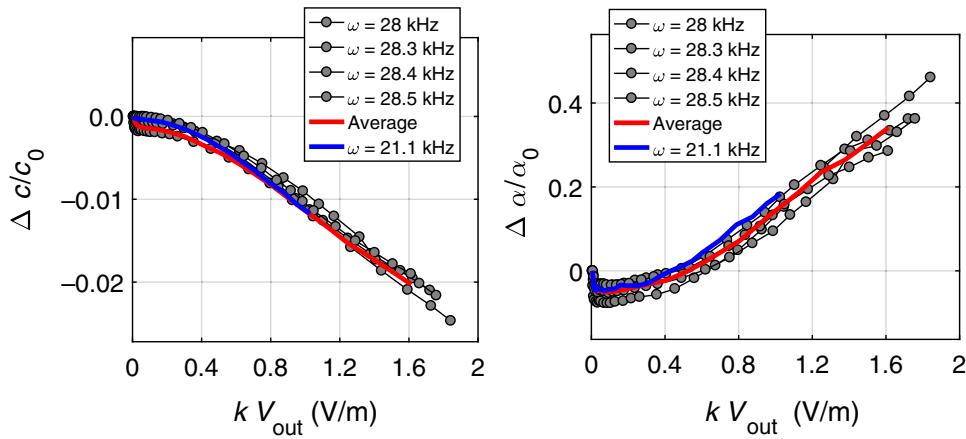


FIG. 4. Velocity and damping variations as a function of the product of wave number and output potential detected at the oscilloscope (proportional to strain amplitude). Results are shown for measurements performed at different testing frequencies using the calibration results reported in Fig. 3.

The relative variations of velocity  $c$  and damping  $\alpha$  with respect to the linear values are shown in Fig. 4 as a function of  $kV_{\text{out}}$  (proportional to strain) where we recall that  $k$  is the wave number and  $V_{\text{out}}$  is the amplitude of the potential detected from the oscilloscope. Linear values are those obtained during calibration and reported in Fig. 3.

Measurements are repeated at different frequencies around the third resonance mode and also close to the

second mode (always using the calibration results discussed in the previous subsection): in agreement with expectations, velocity decreases with increasing amplitude of excitation and damping increases. Variations are small for velocity (a few percent) and much higher for damping (up to 40%). Furthermore, results seem to confirm that in a narrow frequency range of the order of a few kHz elastic nonlinearity for Berea does not depend on frequency [33].

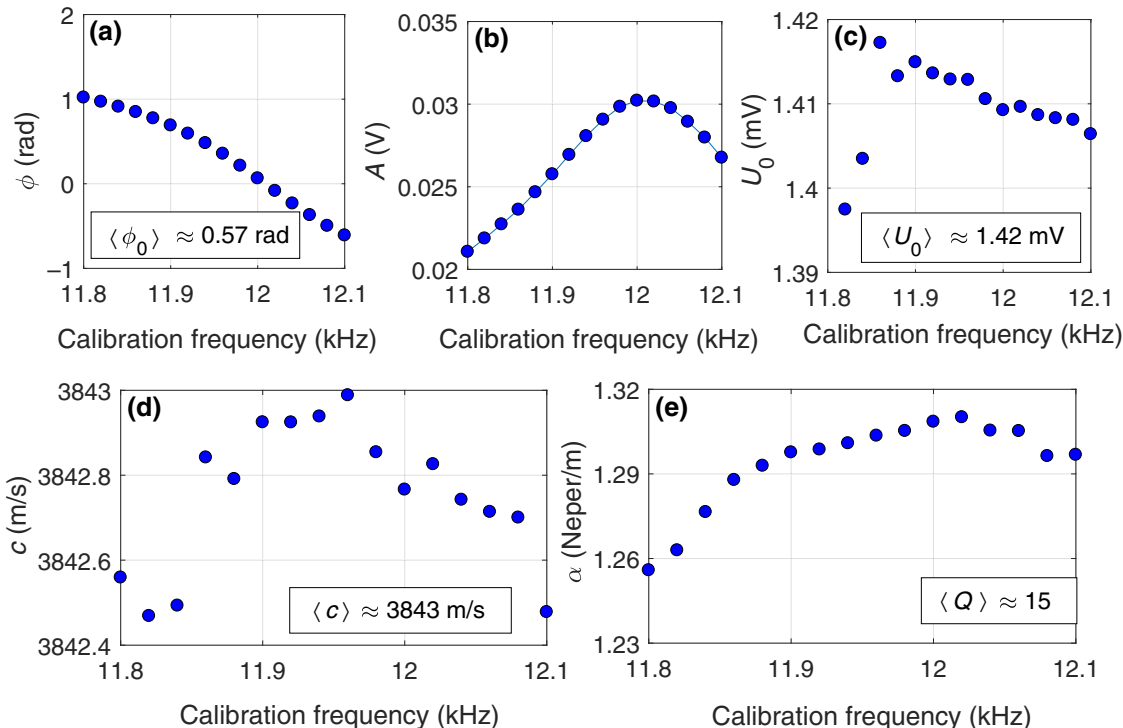


FIG. 5. Results of the calibration procedure performed for the concrete sample B06. All quantities are reported as a function of the calibration frequency. (a) Phases ( $\phi = \Phi - \phi_0$ ); (b) amplitudes ( $A$ ); (c) calibration amplitude ( $U_0$ ); (d) estimated velocity; (e) estimated damping. Distance correlation coefficients [39] are 0.6, 0.45, and 0.62 for  $U_0$ ,  $c$ , and  $\alpha$ , respectively.

Accurate measurements on Berea sandstone using DAET indicate dependence of nonlinear parameters on frequency, but on a much larger frequency range (from Hz to hundreds of kHz) [40].

### C. Concrete and cement-paste samples

#### 1. Calibration, linear velocity, and damping measurement

The same analysis is also conducted for the other tested samples. Calibration is initially performed around a given resonance mode (first mode for sample B06 and third mode for sample B3), to obtain linear velocity and damping. Calibration is again performed at a low amplitude of excitation (20 mV before amplification).

Results, as a function of the calibration frequency, are shown in Figs. 5 and 6. Cement paste and concrete have a higher degree of heterogeneity, which makes calibration less effective. Indeed calibration is not as independent from frequency as in the case of Berea. Distance correlation coefficients (reported in the captions) are slightly higher than in the case of Berea, even though the small statistical ensemble available reduces the significance of any statistical test. The existence of a correlation between calibration parameters and frequency can be meaningful in the case of sample B3, for which we observe in particular a slight increase of damping with frequency, as shown in

(e) of Fig. 6. Measured values for velocity and  $Q$  are in good agreement with results reported in the literature for similar samples [41] in the same frequency range, except for damping in the cement-paste case, in which case  $\alpha$  is 1 order of magnitude smaller than results reported in the literature.

We also note that, as expected, the calibration parameters do not differ significantly for the three samples considered, since an identical experimental setup is used for testing the three materials.

#### 2. Nonlinearity

Using the calibration results, it has been possible to analyze the dependence of velocity and damping on a quantity proportional to strain amplitude, following the same approach described for Berea. Results are shown in Figs. 7 and 8. In the case of sample B3 (cement paste) the sample is tested at two close by frequencies. Nonlinearity in concrete (Fig. 7) is very similar to nonlinearity observed in Berea, while the behavior is slightly different in the case of the cement-paste sample. In both cases, as in Berea, nonlinearity in the damping coefficient is more significant than nonlinearity in velocity. The different behavior of B3 with respect to both Berea and concrete can be due either to microstructural differences between the samples or to effects linked to calibration (which in the case of B3

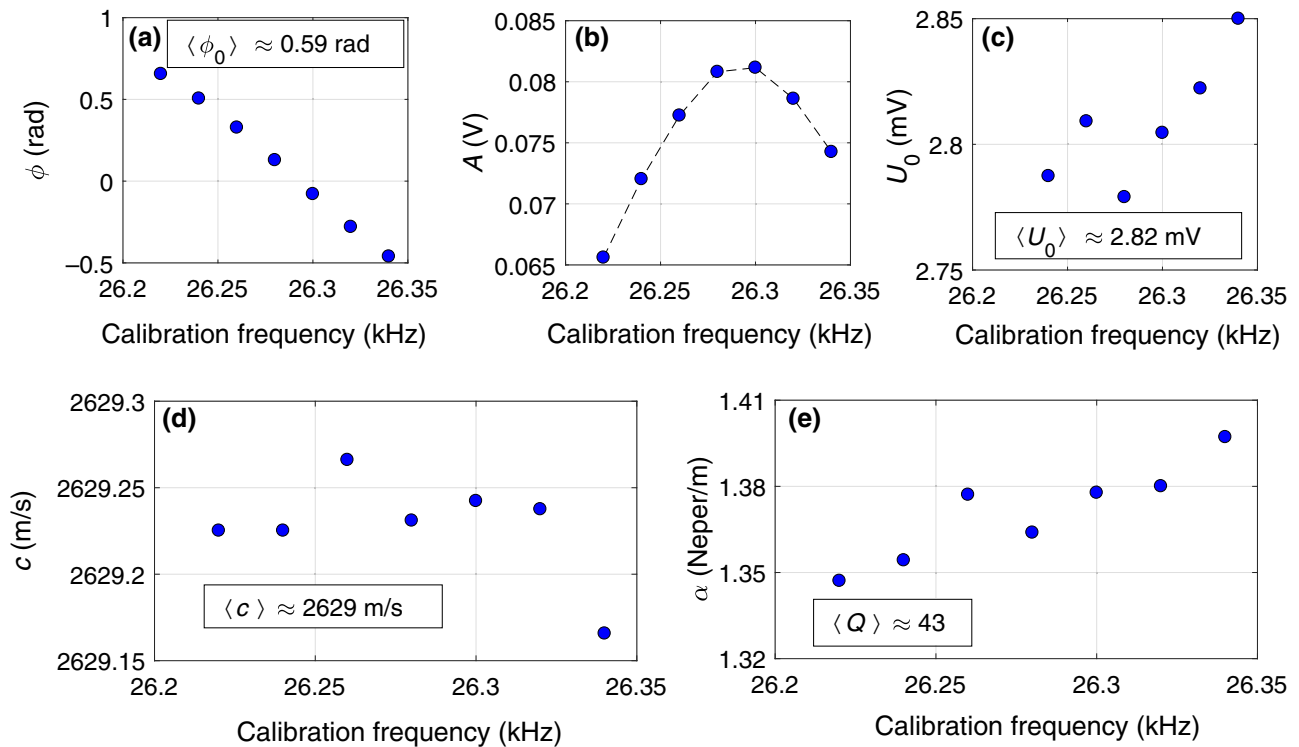


FIG. 6. Results of the calibration procedure performed for the cement-paste sample B3. All quantities are reported as a function of the calibration frequency. (a) Phases ( $\phi = \Phi - \phi_0$ ); (b) amplitudes ( $A$ ); (c) calibration amplitude ( $U_0$ ); (d) estimated velocity; (e) estimated damping. Distance correlation coefficients [39] are 0.7, 0.55, and 0.64 for  $U_0$ ,  $c$ , and  $\alpha$ , respectively.

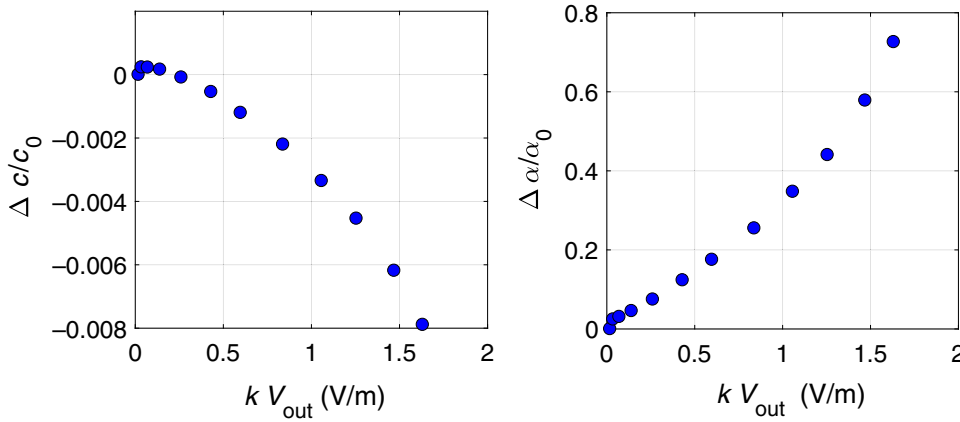


FIG. 7. Velocity and damping variations as a function of the product of wave number and output potential detected at the oscilloscope (proportional to strain amplitude) in the case of sample B06 (concrete). Results are obtained using the calibration results reported in Fig. 5

appeared more frequency dependent than for concrete and Berea). At this stage a further analysis, also considering a statistical ensemble of samples, is needed before being allowed to provide a definitive answer.

#### D. Discussion

Before proceeding to illustrate the potential of the proposed approach for applications, we summarize here the current advantages and limitations of these kinds of measurements. The potentialities of the method, which have already been highlighted, are related to the ease of implementation, the rapidity of the acquisition protocol and the possibility to separate damping from velocity based on a physically grounded solution. Also, experimental observations reported here and in the following, seem to support the robustness of the approach.

As for items that should be further investigated concerning the reliability of the method, and thus can result in limitations to the applicability under some circumstances, we list the following:

(a) The approach works in 1D conditions only. This can not be avoided, while we believe the limitation of using

longitudinal waves can be overcome by finding appropriate solutions for other wave types.

(b) The approach allows determining equivalent velocities or dampings for each excitation amplitude by using a linearized solution. In specific cases in which nonlinearity assumes a well-defined expression, the analytic solution can be modified, e.g., with a perturbation theory approach, but in general this is not feasible. Most of the methods available in the literature suffer from the same limitation since they provide for each amplitude a single value, e.g., of velocity, while indeed the studied quantity varies with time.

(c) Accuracy needed during calibration to obtain a given accuracy of the results have to be carefully investigated. Likewise, the accuracy of the approach should be tested when calibration is not optimal, e.g., manifesting frequency dependence as in the case of one of the samples discussed here.

(d) In nonlinear systems the dependence of velocity and damping on strain amplitude is the relevant function to be determined. At this stage, as in most other techniques, the approach proposed allows us to only define the dependence on a quantity, which is proportional to strain amplitude, thus quantification of the nonlinear parameters could be debatable. This item surely deserves more attention and

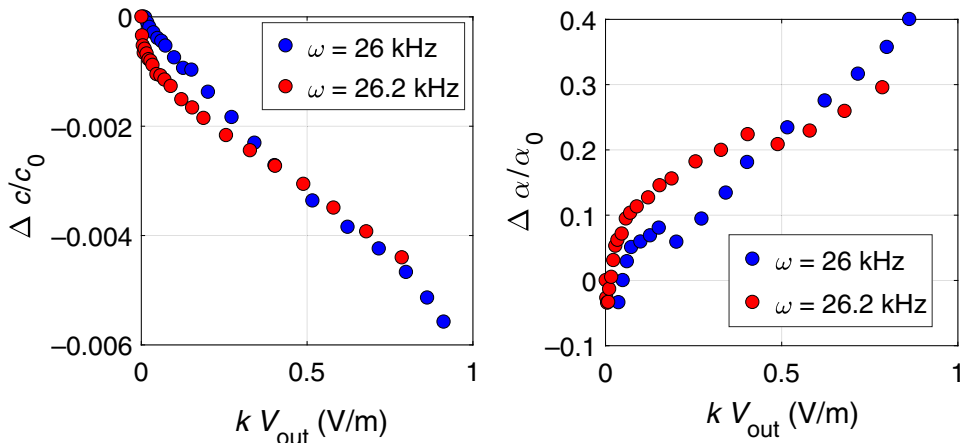


FIG. 8. Velocity and damping variations as a function of the product of wave number and output potential detected at the oscilloscope (proportional to strain amplitude) in the case of sample B3 (cement paste). Results are shown for measurements performed at different testing frequencies using the calibration results reported in Fig. 6.

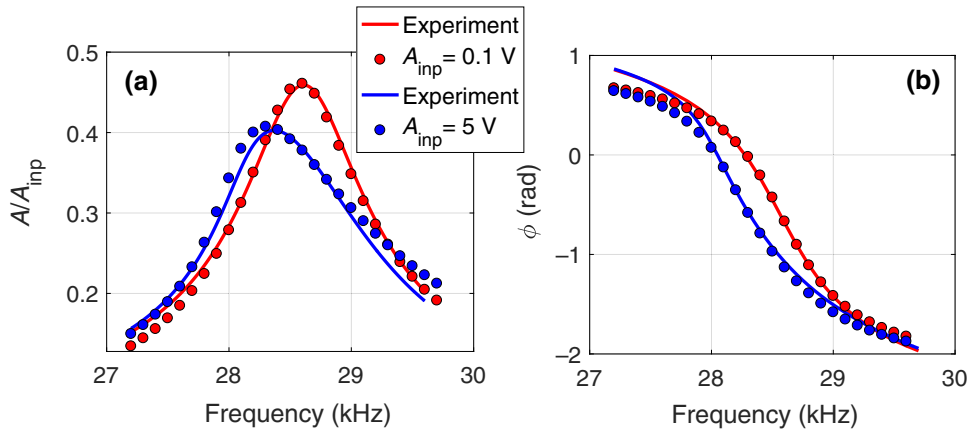


FIG. 9. Berea sandstone. Calculated normalized amplitudes (a) and phases (b) of signals detected for two different values of the excitation amplitude (red and blue dots). The analytical calculation has been carried out using the amplitude dependence of velocity and damping calculated from measurements performed at a single frequency of excitation and reported in Fig. 4. Results obtained are compared with experimental data (solid lines), obtained measuring phases and amplitude of signals varying both input amplitude and frequency (each point corresponding to a measurement).

the possible findings could be beneficial for other methods, which suffer the same limitation.

## V. APPLICATIONS

### A. Resonance frequency shift

Several applications can be envisaged, once the dependencies of velocity and damping factor on amplitude are measured. For instance, we can derive the nonlinear resonance curves. In fact, Eqs. (6) and (7) allow us to derive the amplitude and phases of the signal as a function of frequency and input amplitude  $A_{\text{inp},i} = m_i A_{\text{inp},0}$  ( $i = 1, \dots, n$ ), once the dependence of  $c$  and  $\alpha$  on  $A$  are known. The procedure consists in finding iteratively the solution:

(a) Frequency  $\omega$  and input amplitude  $m_i$  are given; using an initial guess for  $c$  and  $\alpha$  the output amplitude  $A(\omega, m_i)$  and phases  $\phi(\omega, m_i)$  are calculated.

(b) Considering data of Fig. 4 it emerges that the guessed velocity and damping values are not those correct for the given amplitude. Thus, from the curves showing dependence of velocity or damping on amplitude a new guess for  $c$  and  $\alpha$  is determined.

(c) Amplitude and phase are recalculated using the new guess and the procedure is repeated up to convergence.

We first apply the procedure to the Berea sample. Results are shown in Fig. 9 for two selected input amplitudes and are compared with experimental data obtained from direct measurements of phases and amplitudes with repeated

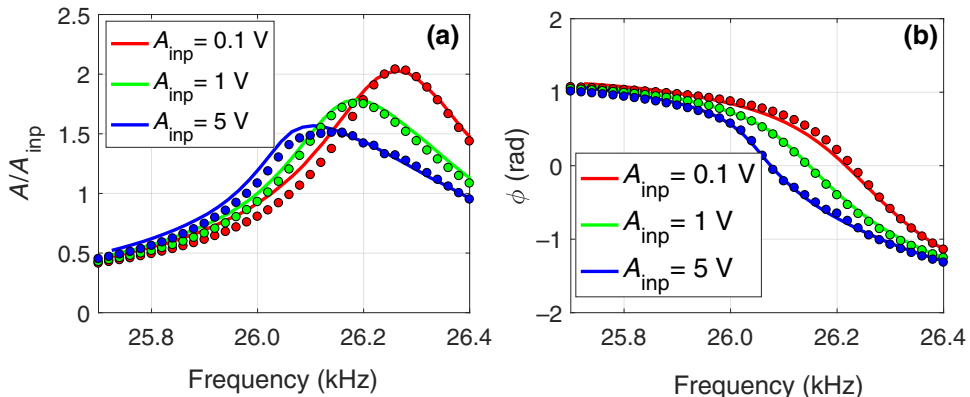


FIG. 10. Concrete sample. Calculated (normalized to input) amplitudes (a) and phases (b) of signals detected for three different values of the excitation amplitude (dots). The analytical calculation has been carried out using the amplitude dependence of velocity and damping calculated from measurements performed at a single frequency of excitation and reported in Fig. 7. Results obtained are compared with experimental data (solid lines), obtained measuring phases and amplitude of signals varying both input amplitude and frequency (each point corresponding to a measurement).

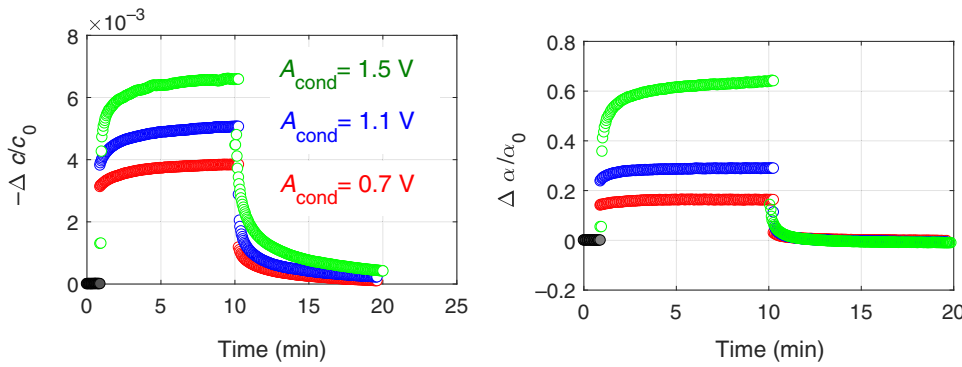


FIG. 11. Evolution in time of velocity and damping measured when conditioning amplitude is on or off. Experiments are conducted at different values of the conditioning amplitude.

experiments injecting monochromatic waves with increasing frequencies. The agreement between the results is excellent. The approach proposed here allows determination of the shift of the resonance frequency with high accuracy, i.e., the softening of the material with increasing amplitude of excitation, and the deformation of the resonance curve at the higher amplitude [see Fig. 9(a)].

Finally, for the concrete sample the curves describing the dependence on amplitude of the physical parameters (velocity and attenuation) are used to predict the resonance curves of the sample at increasing amplitudes of excitation. Results are shown in Fig. 10 for resonance curves at three increasing amplitudes of excitation. We show here results for the second longitudinal mode of the sample (even though calibration and determination of nonlinearity is carried out around the first mode) to prove the robustness of the predictions obtained with our approach. Calculated resonance curves agree well with those measured

experimentally by sweeping frequencies. Resonance down shift, damping increase, and curve distortions are well reproduced by the calculations performed.

## B. Conditioning and relaxation

Memory effects are peculiar of hysteretic elastic media [7,8,34,35] and consist in the following. When a sample is excited at a fixed (high) amplitude of excitation, transition to a nonequilibrium state is observed (conditioning), which is manifested by a not instantaneous change of both velocity and damping. The effect is fully reversible, i.e., when the excitation is removed, slowly in time the system relaxes back to the original state (relaxation).

Full conditioning and relaxation take place on a long time scale: minutes to hours, depending on the material. However, monitoring early stages of the evolution of the physical properties is of great importance to understand

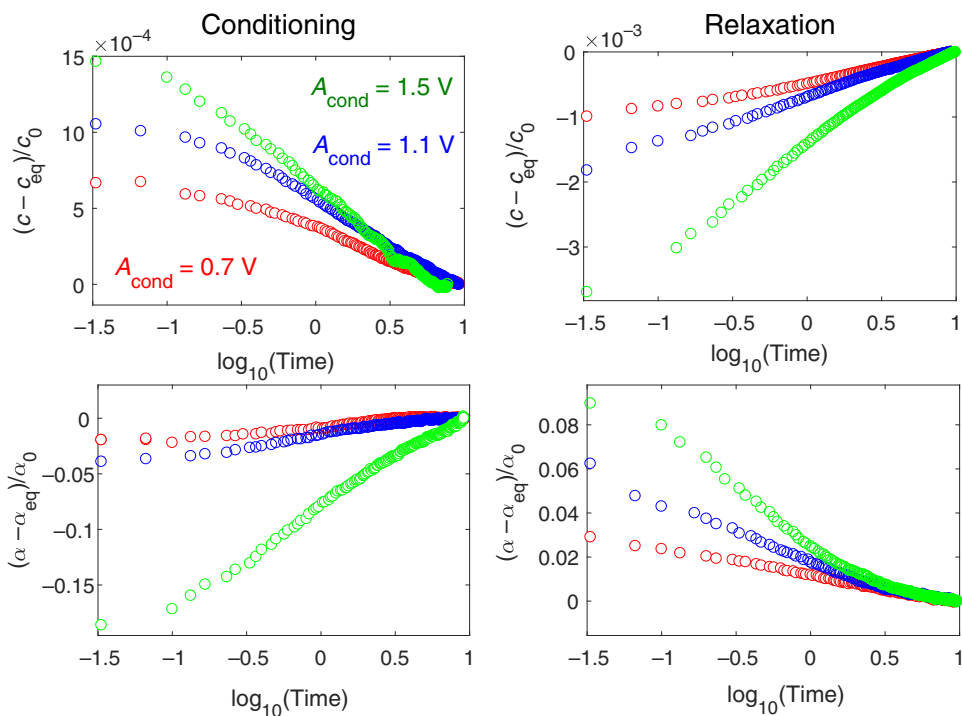


FIG. 12. Evolution in time (logarithmic scale) of velocity and damping measured during conditioning and relaxation. Experiments are conducted at different values of the conditioning amplitude. Same data as Fig. 11.

mechanisms involved in the process, since in the first few minutes of the recovery most of the effects are manifested. The method proposed in this paper is particularly suitable for this purpose, since it allows monitoring in time the independent evolution of velocity and damping with a fast acquisition time. Measurements can indeed be performed almost in real time, with a delay of one or a few seconds between the first measurement and the switching on-off of the conditioning amplitude.

To demonstrate the potential of the approach, the following experiment is conducted on the B06 sample. After calibration (same as reported previously), the sample is excited at a low amplitude of excitation ( $A_{\text{inp}} = A_0 = 0.1$  V). At a given instant, excitation is amplified to a conditioning amplitude  $A_{\text{inp}} = A_{\text{cond}}$  and through successive acquisitions velocity and damping evolution are monitored. Once steady state is reached, amplitude amplification is removed and relaxation of the physical parameters is analyzed.

Results are shown in Fig. 11. As expected, the changes in velocity and damping are not instantaneous and are more and more evident when increasing the amplitude of conditioning. For the considered material, time scales are the same for both quantities and seem to be independent from  $A_{\text{cond}}$ . Almost complete recovery is observed in all cases in the time window considered.

Figure 11 proves the approach proposed here to be suitable for the study of conditioning and relaxation, easy to implement and fast. In Fig. 12 conditioning and relaxation are analyzed separately for the same conditioning amplitudes of Fig. 11. Here a log scale is used for the  $x$  axes, to better appreciate evolution of early stages. In the intermediate time range, the logarithmic-time behavior seems to describe well both conditioning and relaxation [46]. When considering very early (less than about 20 s) or very late (close to equilibrium) stages in the evolution, deviations from the expected behavior are observed, in particular during conditioning. The behavior during both conditioning and relaxation should thus be described by a kinetic law more complex than a simple logarithmic function, such as proposed in Ref. [47].

## VI. CONCLUSIONS

We propose an approach to measure the nonlinearity in velocity and damping coefficient, which is a faster and simpler alternative to standard approaches such as nonlinear elastic wave spectroscopy [10], nonlinear resonant ultrasound spectroscopy [16], or dynamic acoustoelastic testing [25,26]. The method allows independent measurement of the nonlinearity in velocity and damping as the deviation from the linear behavior of “equivalent” linear medium with velocities and damping derived by fitting data. As such, for a given amplitude of excitation we lose the capability of defining nonlinear parameters, e.g., quadratic and cubic coefficients, because the signal itself

is averaging over one strain period and thus providing an averaged response, as in most approaches to measure nonlinearity, except DAET. At the same time, we keep information about both fast and slow dynamics, the latter being the most suitable to be studied with our approach, since its contribution consists in bringing the system to a new linear equilibrium state with a constant in time new equilibrium modulus (or damping), upon which fast dynamic nonlinearity is added. Reliability of the approach is guaranteed only when deviations of output signals from a purely sinusoidal behavior are small, which means weak nonlinearities or weak amplitudes of excitation.

Since the approach is based on measuring phases and amplitudes of signals generated by sinusoidal excitations at a given frequency, measurements can be repeated continuously and in almost “real time,” thus providing an efficient tool, e.g., for monitoring early stages during conditioning and relaxation or for online measurements. Finally, we remark that the short measurement time is one of the main advantages of the proposed approach: during relaxation, e.g., the first measurement can be taken as fast as after a couple of seconds from the end of conditioning, which is to our knowledge faster than any acoustic nonlinear characterization method in the literature.

## APPENDIX A: DERIVATION OF THE SOLUTION IN $x = L$

The solution for the displacement field in a finite medium of length  $L$  with free-free boundary conditions is reported in Eq. (4). When  $x = L$  we obtain

$$\begin{aligned} u^+(x = L, t) &= \sum_{n=1}^{\infty} U_0 e^{j[\omega t - k(2n-1)L + \phi_0]} e^{-\alpha(2n-1)L}, \\ u^-(x = L, t) &= \sum_{n=1}^{\infty} U_0 e^{j[\omega t - k(2n-1)L + \phi_0]} e^{-\alpha(2n-1)L}, \\ u(x = L, t) &= 2U_0 e^{j(\omega t + \phi_0)} \sum_{n=1}^{\infty} e^{-jk(2n-1)L - \alpha(2n-1)L}. \end{aligned} \quad (\text{A1})$$

The index  $n$  can be redefined to have summation from 0:  $m = n - 1$ . It follows that

$$\begin{aligned} u(x = L, t) &= 2U_0 e^{j(\omega t + \phi_0)} \sum_{m=0}^{\infty} e^{-jk(2m+1)L - \alpha(2m+1)L}, \\ u(x = L, t) &= 2U_0 e^{j(\omega t + \phi_0)} e^{-jkL - \alpha L} \sum_{m=0}^{\infty} e^{-j2kmL - \alpha 2mL} \end{aligned} \quad (\text{A2})$$

Defining

$$z = e^{-2jkL - 2\alpha L}, \quad (\text{A3})$$

the summation is a geometric series with  $|z| < 1$ . Thus the series is convergent [32] and

$$\begin{aligned} u(x = L, t) &= 2U_0 e^{j(\omega t + \phi_0)} e^{-jkL - \alpha L} \frac{1}{1 - z}, \\ u(x = L, t) &= U_0 e^{j(\omega t + \phi_0)} \frac{2}{e^{jkL + \alpha L} - e^{-jkL - \alpha L}}, \\ u(x = L, t) &= U_0 e^{j(\omega t + \phi_0)} \frac{1}{\sinh(jkL + \alpha L)}. \end{aligned} \quad (\text{A4})$$

Defining

$$\begin{aligned} q &= \sinh(jkL + \alpha L), \\ q &= \sinh(\alpha L) \cos(kL) + j \cosh(\alpha L) \sin(kL), \end{aligned} \quad (\text{A5})$$

we obtain

$$\frac{1}{\sinh(jkL + \alpha L)} = \frac{1}{\sqrt{\cosh^2(\alpha L) - \cos^2(kL)}} e^{-j \arctan[\tan(kL)/\tanh(\alpha L)]}. \quad (\text{A6})$$

Introducing Eq. (A6) into Eq. (A4), we obtain the displacement field in  $x = L$  as

$$u(x = L, t) = \frac{U_0}{\sqrt{\cosh^2(\alpha L) - \cos^2(kL)}} e^{j(\omega t + \phi_0 - \arctan[\tan(kL)/\tanh(\alpha L)])}, \quad (\text{A7})$$

as reported in the main text.

## APPENDIX B: STRAIN

In the main text, it is chosen to derive the solution in terms of displacements. However, a similar solution can be derived for strain:

$$\partial u / \partial x \approx (-jk - \alpha)u(x, t), \quad (\text{B1})$$

where the approximation is due to neglecting the effects of viscous terms on phase. In practice, such a choice is equivalent to redefining the calibration parameters  $U_0$  and  $\phi_0$ , without significant modifications to the approach proposed.

The advantage of an approach based on strains, is that it allows an easier expression of the free-free boundary conditions and a better physical understanding of the coefficient  $U_0$ . Indeed, boundary conditions become

$$\begin{aligned} \frac{\partial u}{\partial x} &= 0 \quad \text{at } x = L, \\ \frac{\partial u}{\partial x} &= (-jk - \alpha)U_0 e^{j(\omega t + \phi_0)} \quad \text{at } x = 0 \end{aligned}$$

The second boundary condition corresponds to that of free-free boundaries plus the contribution due to the strain induced by the source transducer.

## APPENDIX C: BOUNDARY CONDITIONS

The solution given in the main text is exact for a finite linear medium with free-free boundary conditions, which can not be the case of the experimental setup. However, considering two small and light piezoelectric ultrasonic transducers bounded to the edges of a 1D sample positioned horizontally, to avoid gravity effects, and on a soft surface (foam rubber in our case) or suspended, the boundary conditions are normally considered to approximate well a free-boundary system (see, e.g., [33–35]). In our case, we measure the velocity and  $Q$  factor for the Berea sandstone sample independently on the use of our technique and find that the obtained measurements agree well with those obtained assuming free-free boundary conditions in our model, as shown in Fig. 3. Thus, even though small effects due to the transducer's mass might be present, we can consider them negligible.

Even in the case of other boundary conditions, it is possible to modify the approach, considering a reflection coefficient  $R$  and a phase change  $\Delta\Phi$  due to boundaries. Considering only the  $u^+$  term, Eq. (4) can be rewritten as

$$u^+(x, t) = \sum_{n=1}^{\infty} U_0 R^{2(n-1)} e^{j\{\omega t - k[2(n-1)L+x] + 2(n-1)\Delta\Phi + \phi_0\}} e^{-\alpha[2(n-1)L+x]},$$

which can still be solved to obtain a sinusoidal solution. In fact, in  $x = L$  we obtain

$$u^+(x = L, t) = e^{-j\Delta\Phi - \log(R)} \sum_{n=1}^{\infty} U_0 e^{j\{\omega t - k'[(2n-1)L] + \phi_0\}} e^{-\alpha'[2(n-1)L]},$$

where

$$\begin{aligned} k' &= k - \Delta\Phi/L, \\ \alpha' &= \alpha - \log(R)/L. \end{aligned} \quad (\text{C1})$$

The sum is in most cases still convergent [since  $\log(R) < 0$ ], albeit with more complex calculations. Furthermore, the presence of the two additional unknown parameters  $R$  and  $\Delta\Phi$ , makes the procedure more complex, e.g., requiring to obtain them by fitting the linear values of velocity and  $Q$  factor, but still feasible.

## APPENDIX D: WAVE NUMBER AND DAMPING COEFFICIENT DETERMINATION

In the main text, equations are reported linking measured phases and amplitudes of the signal to wave number  $k$  and damping  $\alpha$ :

$$A = \frac{U_0}{\sqrt{\cosh^2(\alpha L) - \cos^2(kL)}}, \quad (\text{D1})$$

$$\Phi = \phi_0 + \phi = \phi_0 - \arctan \left[ \frac{\tan(kL)}{\tanh(\alpha L)} \right]. \quad (\text{D2})$$

These equations can be easily inverted. Introducing the new variables  $a = \tanh(\alpha L)$  and  $b = \tan(kL)$ , we obtain

$$\frac{A^2}{U_0^2} \times \left( \frac{1}{1-a^2} + \frac{1}{1+b^2} \right) = 1, \quad (D3)$$

$$b = -a \tan(\Phi - \phi_0) = -a \tan(\Delta\Phi).$$

Substituting  $b$  in the first equation, we have a second-order equation in  $a^2$ :

$$a^4 \sin^2 \Delta\Phi + a^2 \left[ \frac{A^2}{U_0^2} + \cos(2\Delta\Phi) \right] - \cos^2 \Delta\Phi = 0 \quad (D4)$$

The equations reported in the text follows from the solution of Eq. (D4).

- 
- [1] A. A. Shah and Y. Ribakov, Non-destructive evaluation of concrete in damaged and undamaged states, *Mater. Des.* **30**, 3504- (2009).
  - [2] P. Antonaci, C. L. E. Bruno, P. G. Bocca, M. Scalerandi, and A. S. Gliozzi, Nonlinear ultrasonic evaluation of load effects on discontinuities in concrete, *Cem. Concr. Res.* **40**, 340- (2010).
  - [3] R. A. Guyer, J. Tencate, and P. A. Johnson, Hysteresis and the dynamic elasticity of consolidated granular materials, *Phys. Rev. Lett.* **82**, 3280- (1999).
  - [4] J. Riviere *et al.*, A set of measures for the systematic classification of the nonlinear elastic behavior of disparate rocks, *J. Geoph. Res. Solid Earth* **120**, 1587- (2015).
  - [5] V. Y. Zaitsev, V. E. Gusev, V. Tournat, and P. Richard, Slow Relaxation and Aging Phenomena at the Nanoscale in Granular Materials, *Phys. Rev. Lett.* **112**, 108302 (2014).
  - [6] I. Solodov and G. Busse, Resonance ultrasonic thermography: Highly efficient contact and air-coupled remote modes, *Appl. Phys. Lett.* **102**, 061905 (2013).
  - [7] J. A. TenCate, D. Pasqualini, S. Habib, K. Heitmann, D. Higdon, and P. A. Johnson, Nonlinear and nonequilibrium dynamics in geomaterials, *Phys. Rev. Lett.* **93**, 065501 (2004).
  - [8] M. Scalerandi, A. S. Gliozzi, C. L. E. Bruno, and P. Antonaci, Nonequilibrium and hysteresis in solids: Disentangling conditioning from nonlinear elasticity, *Phys. Rev. B* **81**, 104114 (2010).
  - [9] M. Scalerandi, M. Bentahar, and C. Mechri, Conditioning and elastic nonlinearity in concrete: Separation of damping and phase contributions, *Constr. Build. Mater.* **161**, 208- (2018).
  - [10] K. van den Abeele and J. DeVisscher, Damage assessment in reinforced concrete using spectral and temporal nonlinear vibration techniques, *Cem. Concr. Res.* **30**, 1453- (2000).
  - [11] M. Scalerandi, A. S. Gliozzi, C. L. E. Bruno, D. Masera, and P. Bocca, A scaling method to enhance detection of a nonlinear elastic response, *Appl. Phys. Lett.* **92**, 101912 (2008).
  - [12] G. Kim *et al.*, Drying shrinkage in concrete assessed by nonlinear ultrasound, *Cem. Concr. Res.* **92**, 16 (2017).
  - [13] M. Ait Ouarabi *et al.*, Nonlinear coda wave analysis of hysteresis in strongly scattering elastic media, *Phys. Rev. B* **94**, 134103 (2016).
  - [14] T. J. Ulrich *et al.*, Application of nonlinear dynamics to monitoring progressive fatigue damage in human cortical bone, *Appl. Phys. Lett.* **91**, 213901 (2007).
  - [15] A. S. Gliozzi, M. Scalerandi, G. Anglani, P. Antonaci, and L. Salini, Correlation of elastic and mechanical properties of consolidated granular media during microstructure evolution induced by damage and repair, *Phys. Rev. Mat.* **2**, 013601 (2018).
  - [16] P. A. Johnson, B. Zinsner, and P. N. J. Rasolofosaon, Resonance and elastic properties in rock, *J. Geoph. Res. Sol. Earth* **101**, 11553 (1996).
  - [17] K. E. A. van den Abeele *et al.*, Nonlinear elastic wave spectroscopy techniques to discern material damage, part II: single-mode nonlinear resonance acoustic spectroscopy, *Res. Nond. Eval.* **12**, 31 (2000).
  - [18] S. Haupert *et al.*, High-accuracy acoustic detection of non-classical components of material nonlinearity, *J. Acoust. Soc. Am.* **130**, 2654 (2011).
  - [19] J. Chen, J. Y. Kim, K. E. Kurtis, and L. J. Jacobs, Theoretical and experimental study of the nonlinear resonance vibration of cementitious materials with an application to damage characterisation, *J. Acoust. Soc. Am.* **130**, 2728 (2011).
  - [20] V. Tournat and V. Gusev, Nonlinear effects for coda-type elastic waves in stressed granular media, *Phys. Rev. E* **80**, 011306 (2009).
  - [21] M. Scalerandi *et al.*, Evidence of microstructure evolution in solid elastic media based on a power law analysis, *Comm. Nonlin. Sci. Num. Simul.* **22**, 334 (2015).
  - [22] V. Aleshin and K. van den Abeele, Hertz-Mindlin problem for arbitrary oblique 2D loading: General solution by memory diagrams, *J. Mech. Phys. Solids* **60**, 14 (2012).
  - [23] G. Shkerdin and C. Glorieux, Nonlinear modulation of Lamb modes by clapping delamination, *J. Acoust. Soc. Am.* **124**, 3397- (2008).
  - [24] C. Pecorari, Adhesion and nonlinear scattering by rough surfaces in contact: Beyond the phenomenology of the Preisach-Mayergoz framework, *J. Acoust. Soc. Am.* **116**, 1938 (2004).
  - [25] G. Renaud *et al.*, Nonlinear elastodynamic in microinhomogeneous solids observed by head-wave based dynamic acoustoelastic testing, *J. Acoust. Soc. Am.* **130**, 3583- (2011).
  - [26] J. Rivière, G. Renaud, R. A. Guyer, and P. A. Johnson, Pump and probe waves in dynamic acousto-elasticity: Comprehensive description and comparison with nonlinear elastic theories, *J. Appl. Phys.* **114**, 054905 (2013).
  - [27] C. Trarieux *et al.*, Modeling nonlinear viscoelasticity in dynamic acoustoelasticity, *Appl. Phys. Lett.* **105**, 264103 (2014).
  - [28] M. Scalerandi, A. S. Gliozzi, M. Ait Ouarabi, and F. Boubenider, Continuous Waves Probing in Dynamic AcoustoElastic Testing, *Appl. Phys. Lett.* **108**, 214103 (2016).

- [29] G. G. Stokes, On the theories of internal friction of fluids in motion and of the equilibrium and motion of elastic solids, *Trans. Cambridge Philos. Soc.* **8**, 287 (1849).
- [30] O. O. Vakhnenko, V. O. Vakhnenko, T. J. Shankland, and J. A. Ten Cate, Strain-induced kinetics of intergrain defects as the mechanism of slow dynamics in the nonlinear resonant response of humid sandstone bars, *Phys. Rev. E* **70**, 015602(R) (2004).
- [31] O. O. Vakhnenko, V. O. Vakhnenko, and T. J. Shankland, Soft-ratchet modeling of end-point memory in the nonlinear resonant response of sedimentary rocks, *Phys. Rev. B* **71**, 174103 (2005).
- [32] <http://www.math.wisc.edu/~M321/complex.pdf>.
- [33] M. Remillieux *et al.*, Decoupling Nonclassical Nonlinear Behaviour of Elastic Wave Types, *Phys. Rev. Lett.* **116**, 115501 (2016).
- [34] M. Lott *et al.*, Nonlinear elasticity in rocks: A comprehensive three-dimensional description, *Phys. Rev. Mat.* **1**, 023603 (2017).
- [35] M. Bentahar *et al.*, Hysteretic elasticity in damaged concrete: Quantitative analysis of slow and fast dynamics, *Phys. Rev. B* **73**, 014116 (2006).
- [36] R. A. Guyer and P. A. Johnson, *Nonlinear Mesoscopic Elasticity* (Wiley-VCH, Weinheim, 2009), Chap. 3.
- [37] K. W. Winkler, Dispersion analysis of velocity and attenuation in Berea sandstone, *J. Geoph. Res.* **90**, 6793 (1986).
- [38] C. McCann and J. Sothcott, Sonic to ultrasonic  $Q$  of sandstones and limestones: Laboratory measurements at in situ pressures, *Geophysics* **74**, WA93 (2009).
- [39] G. J. Szekely, M. L. Rizzo, and N. K. Bakirov, Measuring and testing dependence by correlation of distances, *Ann. Stat.* **35**, 2769 (2007).
- [40] J. Riviere *et al.*, Frequency, pressure and strain dependence of nonlinear elasticity in Berea sandstone, *Geoph. Res. Lett.* **43**, 3226 (2016).
- [41] T. P. Philippidis and D. G. Aggelis, Experimental study of wave dispersion and attenuation in concrete, *Ultrasonics* **43**, 584 (2005).
- [42] S. M. Hogg *et al.*, Nonlinear resonant ultrasound spectroscopy of stress corrosion cracking in stainless steel rods, *NDT & E Int.* **102**, 194- (2019).
- [43] S. Ghahramani *et al.*, Monitoring the Carbonation-Induced Microcracking in Alkali-Activated Slag (AAS) by Nonlinear Resonant Acoustic Spectroscopy (NRAS), *Adv. Civ. Eng. Mat.* **7**, 576- (2018).
- [44] P. Shokouhi *et al.*, Dynamic acousto-elastic testing of concrete with a coda-wave probe: Comparison with standard linear and nonlinear ultrasonic techniques, *Ultrasonics* **81**, 59- (2017).
- [45] J. H. Kim *et al.*, Nonlinear Resonance Vibration Assessment to Evaluate the Freezing and Thawing Resistance of Concrete, *Materials* **12**, 325 (2019).
- [46] J. Tencate, E. Smith, and R. A. Guyer, Universal slow dynamics in granular solids, *Phys. Rev. Lett.* **85**, 1020 (2000).
- [47] R. Snieder, C. Sens-Schonfelder, and R. Wu, The time dependence of rock healing as a universal relaxation process, a tutorial, *Geoph. J. Int.* **208**, 1 (2016).